Chemical Physics Letters 676 (2017) 18–24

Contents lists available at ScienceDirect

Chemical Physics Letters

journal homepage: www.elsevier.com/locate/cplett

Research paper

Water-soluble Au_{13} clusters protected by binary thiolates: Structural accommodation and the use for chemosensing

Weihua Ding [a,b], Chuanqi Huang [b,c,d], Lingmei Guan [a], Xianhu Liu [a,b], Zhixun Luo [a,b,*], Weixue Li [c,d,*]

[a] State Key Laboratory for Structural Chemistry of Unstable and Stable Species, Institute of Chemistry, Chinese Academy of Sciences, Beijing 100190, PR China
[b] Graduate University of Chinese Academy of Sciences (GUCAS), Beijing 100049, PR China
[c] State Key Laboratory of Catalysis, Dalian Institute of Chemical Physics, Chinese Academy of Sciences, Dalian 116023, PR China
[d] School of Chemistry and Material Science, University of Science and Technology of China, Hefei, PR China

ARTICLE INFO

Article history:
Received 17 January 2017
Revised 10 March 2017
In final form 13 March 2017
Available online 15 March 2017

Keywords:
Au_{13} MPCs
Binary thiolates
NBO analysis
Chemosensing
Bioimaging

ABSTRACT

Here we report a successful synthesis of water-soluble 13-atoms gold clusters under the monolayer protection of binary thiolates, glutathione and penicillamine, under a molecular formula of $Au_{13}(SG)_5(PA)_7$. This monolayer-protected cluster (MPC) finds decent stability and is demonstrated to possess an icosahedral geometry pertaining to structural accommodation in contrast to a planar bare Au_{13} of local minima energy. Natural bond orbital (NBO) analysis depicts the interaction patterns between gold and the ligands, enlightening to understand the origin of enhanced stability of the Au_{13} MPCs. Further, the water-soluble Au_{13} MPCs are found to be a decent candidate for chemosensing and bioimaging.

1. Introduction

Gold clusters in recent decades have stimulated extensive research interest owing to their size-dependent properties and promising applications in nanoelectronics, catalysis, chemical sensing, optics and biomedicine, etc. [1–4]. In recent years, a series of monolayer-protected gold clusters (Au MPCs) with precise atomic-level structure have been reported, such as Au_{102} [5], Au_{60} [6], Au_{55} [7], Au_{38} [8], Au_{36} [9,10], Au_{30} [10,11], Au_{25} [12,13], Au_{20} [14,15], and Au_{18} [16], etc. Among others, reasonable research interest has been attracted upon ultrasmall gold clusters at n = 11–13 pertaining to a transition from 2D to 3D structures. In particular, 13-atoms metal clusters (such as Al_{13}^-) enable a minimal icosahedron structure and may fulfill a geometrical shell closing of 40 valence electrons known as a magic number [2,17]. In previously published investigations, gas-phase chemistry and topologies of Al_{13} [18,19], Pt_{13} [20], Ag_{13} [21,22], and Au_{13} clusters [17,23] have been established. According to these reports, icosahedral structures are found to be the most stable for Al_{13} and Pt_{13}, but Ag_{13} bears a bilayer triangular structure. In contrast, Au_{13} was found to have a planar geometry in its lowest-energy ground-state due to covalent bondings of gold atoms [24–28]. However, relativistic effect and electronegativity of the gold atoms perplex the interactions between ligands and gold cores in ligand-protected gold clusters [29–32], which also allows for an icosahedral innermost Au_{13} core for Au MPCs such as the aforementioned Au_{25} [12,13,33]. Therefore, it is important to rationalize the electronic and geometric structures of the typical small gold cluster—Au_{13} MPCs, hence furthering the understanding of the stability of such clusters in gas phase and in wet synthesis [34,35].

Along with the novel gold cluster stability, it's worth mentioning that the urgent demand of biocompatible use of such stable metal clusters has attracted many interests. However, the use of organic solvent as protecting ligand gives rise to poor water solubility of MPCs, which restricts the potential applications of gold clusters in biological systems and environmental analyses. This inconvenience can be overcome by using hydrophilic thiol molecules with diverse functional groups as the ligands to synthesize the water-soluble and biocompatible MPCs, such as glutathione (GSH), D-penicillamine (DPA), 1-thioglycerol, 2-mercaptoethylamine, etc. [36–39]. Among them, GSH is an important antioxidant (tripeptide) capable of preventing damage to cellular components by reactive oxygen species. DPA is a medication (L-penicillamine is toxic) of the chelator class and has also been found an efficient protection ligand in synthesizing nanoclusters with remarkable fluorescence. In addition to the combined consideration of biocompatibility, fluorescence and chelating

* Corresponding authors at: State Key Laboratory for Structural Chemistry of Unstable and Stable Species, Institute of Chemistry, Chinese Academy of Sciences, Beijing 100190, PR China.
E-mail address: zxluo@iccas.ac.cn (Z. Luo).

http://dx.doi.org/10.1016/j.cplett.2017.03.036
0009-2614/

effect, we are also motivated by noting that heterothiolate-protected nanoclusters could give rise to multifold properties [40,41].

Herewith we report a successful synthesis of water-soluble Au_{13} MPCs via the ligand-induced etching method by using a mixed thiolate protection (i.e., penicillamine and glutathione). The cluster structure $Au_{13}(SG)_5(PA)_7$ was determined via high resolution mass spectrometry along with first-principles optimization calculations. Considering the as-prepared Au_{13} MPCs bear decent red fluorescence at 690 nm, we have applied for chemo-sensing in ions detection and bioimaging. It is found that this water-soluble Au_{13} clusters protected by binary thiolates are highly efficient to detect and differentiate Fe^{3+} and Cu^{2+} ions in water and in living cells. This is an important promotion although such ion detection is not a fresh topic. Note that metal ions (such as Fe^{3+}, Cu^{2+}, Mn^{2+}, Cd^{2+}, Hg^{2+} and Pb^{2+} ions) may selectively cause health issues but accurate detection of them is actually not trivial, especially in vivo.

2. Experimental section

2.1. Chemicals

Hydrogen tetrachloroaurate(III), hydrate (49% Au) was purchased from Alfa Aesar. L-glutathione (reduced, 99%), penicillamine and sodium borohydride (99%) were obtained from J&K Scientific Ltd. (Beijing, China). Methanol (HPLC purity) was purchased from Sinopharm Chemical Reagent Co., Ltd. (Beijing, China). Ultrapure water (18.2 MΩ) was used in all experiments.

2.2. Synthesis of Au MPCs

All chemicals (analytical and spectroscopic grade) were commercially available and used as received without further purification. The monolayer-protected gold clusters were synthesized according to the following procedure. Firstly, the aqueous solution of H_4AuCl_3 (98.46 mg, 0.25 mM) and glutathione (GSH; 307.32 mg, 1.0 mM) were mixed together in the solution and kept at ~0 °C in an ice bath for 30 min. To this clear solution, a freshly prepared ice-cold aqueous $NaBH_4$ (94.58 mg, 12.5 mL) were slowly added dropwise under vigorous stirring condition. After removing the ice bath, the reaction was allowed to proceed under constant stirring for 1 h, and the products were precipitated with methanol. After filtration, black precipitate of Au nanoparticles (Au NPs) were obtained, and then washed with excessive methanol. Secondly, the as-prepared Au NPs were dissolved and stabilized in 12.5 mL H_2O. After penicillamine (PA, 74.6 mg, 0.5 mM) slowly added dropwise to the solution, the reaction was allowed to proceed under constant stirring for 12 h at 55 °C. The final gold clusters were precipitated and filtration with methanol.

3. Results and discussion

We used high-resolution electrospray ionization mass spectrometry (ESI MS) to monitor and optimize the synthesis of the as-prepared gold clusters, as shown in Fig. 1A, where an intense peak at $m/z = 2562.68359$ was observed (marked as peak No. 1), exclusively assigned to $[Au_{13}(SG)_5(PA)_7]^{2-}$ along with identical isotopic distributions comparing with simulated pattern (Fig. 1A inset). This specific isotope pattern ensures exclusive identification of the as-prepared cluster. There are also a few other sodium-involved [1,42,43] and MeOH-attached peaks showing reasonable intensity due to the mobile phase molecules, such as $[Au_{13}(SG\text{-}H)_5(PA)_7Na]^{2-}$ (No. 2, 2573.67682), $[Au_{13}(SG\text{-}2H)_5(PA)_7Na_2(CH_3OH)]^{2-}$ (No. 3, 2601.25619), $[Au_{13}(SG\text{-}3H)_5(PA)_7Na_3(CH_3OH)]^{2-}$ (No. 4, 2601.25619) and $[Au_{13}(SG\text{-}2H)_5(PA)_7Na_2(CH_3CN)(CH_3OH)]^{2-}$ (No. 5, 2637.21145), evidencing the Au_{13} motifs synthesized in our procedure. More characterization details (UV–Vis adsorption, TEM, XPS and fluorescence spectrum) as well as the expanded and simulated spectra of these fragment peaks are given in Figs. S1–S3 (ESI). The polyacrylamide gel electrophoresis (PAGE) analysis reveals high grade of purity of the Au_{13} MPCs (Fig. S2d, ESI).

Fig. 1B presents a FT-IR spectrum of the Au_{13} MPCs comparing with that of glutathione and penicillamine respectively. It is worth noting that the infrared-active mode assigned to S—H bond vibration disappears in the Au_{13} MPCs, indicating a substitute of the S—H bond by corresponding Au—S bond in forming the protected monolayer. To further investigate the ligand binding mode on the surface, 2D-NMR correlation (^1H-^1H COSY) experiment was conducted, as shown in Fig. 1C, where the peaks are assigned as the proton signals H_a, H_b, H_c on —PA ligands, and H_1-H_6 on —SG ligands. The peaks of H_3 and H_4 proton signals split into two pairs of peaks (labeled as 3, 3′ and 4, 4′). The NMR spectrum shows that —PA and —SG ligands adopt two binding modes on the Au_{13} MPCs surface as the inset shows.

Having measured the formula weight and composition of the Au_{13} MPCs, we then endeavor to fully demonstrate the packing structure of this cluster. Extensive investigations of thiolate-protected metal clusters have ascertained two favorable forms of the lowest-energy structures, i.e., in the form of RS-Au and RS–Au–SR motifs. Furthermore, previously published work has found four lowest-energy geometrical structures for a bare Au_{13}: planar, flake, cuboctahedral, and icosahedral, as shown in Fig. 2A [24–28]. Our calculation results based on both DFT with Gaussian and VASP packages (details of calculation methods in ESI) confirmed that the planar structure of Au_{13} possess a local minimum energy with the others in the following order: E(planar) < E(flake) < E(cuboctahedron) < E(icosahedron), which is in agreement with previous studies [24–28]. However, it is found that the local minimum energy structure of $Au_{13}(SCH_3)_{12}$ belongs to the icosahedral geometry (i.e., one center Au atom and the other 12 Au atoms forming an icosahedral structure). This is consistent with the previous findings of ligand-protected Au_{13} clusters as determined by single-crystal analysis [44,45], indicating the 12 surface sites of an icosahedral Au_{13} are equally favorable for the monolayer protection [46]. It is also evidenced that, from the IR spectroscopic analysis as mentioned above, IR-active mode assigned to S—H bond vibration disappeared, revealing that the 12 ligands chemisorb on the gold core with end-on orientation of the S atoms by forming 12 Au—S bonds. Note that, the average Au—Au bond length of each $Au_{13}(SCH_3)_{12}$ increases comparing to that of a bare Au_{13} (Table S1 in ESI). Furthermore, the UV–Vis absorption spectrum in aqueous solution is reproduced (with identical spectral profile and peak positions) through TD-DFT calculations by using the icosahedral structure of $Au_{13}(SCH_3)_{12}$ as the model system (Fig. S4a, ESI). The theoretical absorption spectrum shows a broad weak absorption band, which appears to be in good agreement with the experimental results, and validates the icosahedral structure of Au_{13} MPCs in the form of RS–Au.

We have also investigated the surface charge distributions typically for cuboctahedral and icosahedral isomers, and find that the charge-density becomes more positively addressed for the core Au atom and more negatively for the surface Au atoms when linked with the ligands (Fig. S5 in ESI). This seems contradictory with the aforementioned lengthening of Au—Au bond when considering that positive and negative charges between the Au atoms might make bonds shorter under coulomb attraction. However, the fact is that, within such an Au—Au—S system, the bond strength of Au—S bond (4.34 eV) is even more intensive than the Au—Au bond (~2.27 eV). NBO analysis shows that it is the electron transfer from ligands to Au—Au bonds that creates strong Au—S covalent bonds

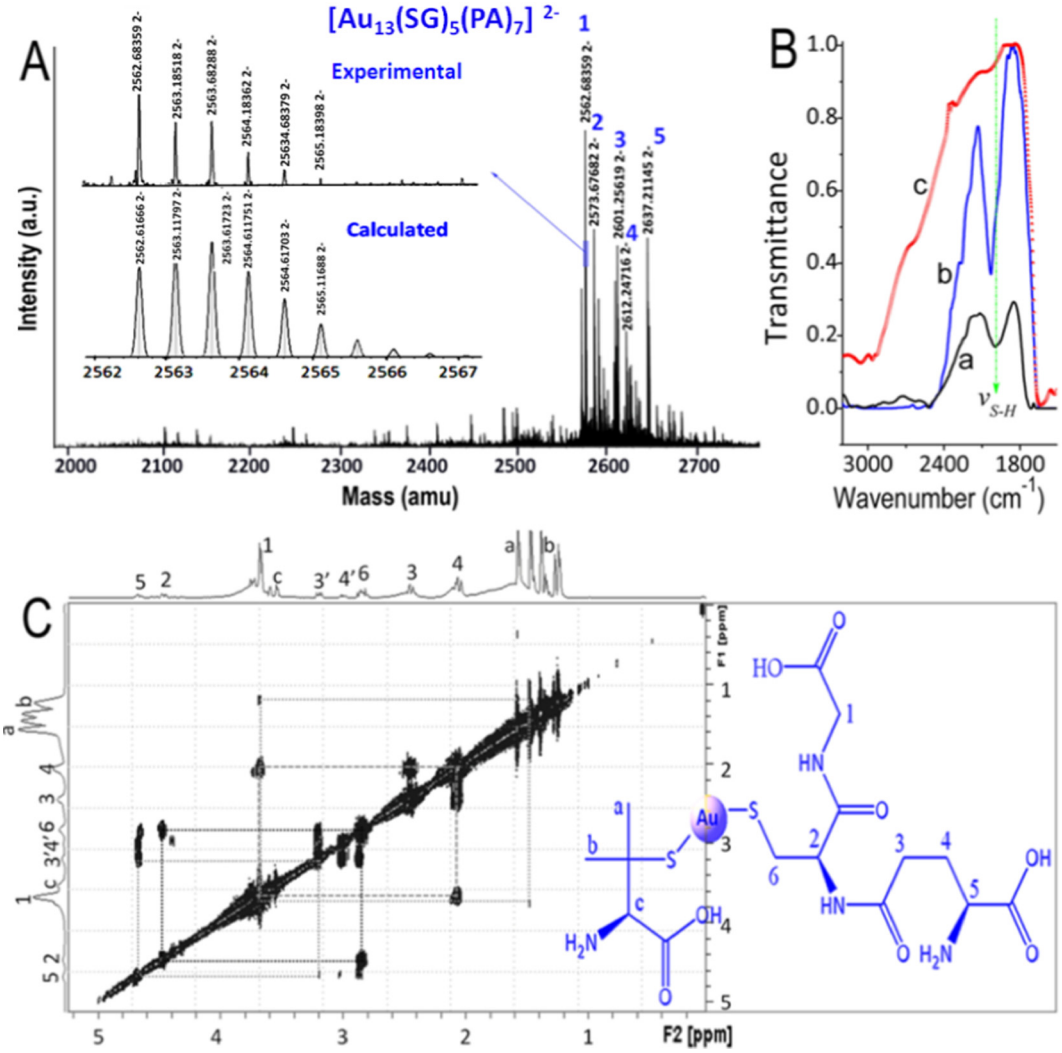

Fig. 1. (A) ESI-MS of the as-prepared gold clusters collected in a negative mode. The inset shows the experimental and simulated isotopic patterns of $[Au_{13}(SG)_5(PA)_7]^{2-}$ cluster. (B) IR spectrum of glutathione (a), penicillamine (b) and the as-prepared Au_{13} MPCs (c). (C) NMR spectra of Au_{13} clusters, where the carbon atoms in glutathione are labeled by the numbers 1–6, while in DPA they are labeled by a, b and c, as seen of the inset on the right.

and leads to elongation of Au—Au bonds. The strong Au—S bonding interactions are also accompanied with large ionization energies as plotted in Fig. 2C where $Au_{13}(SCH_3)_{12}$ is modeled in place of —SR groups [47].

In addition to the large ionization energies for these $Au_{13}(SCH_3)_{12}$ clusters, binding energies and HOMO-LUMO gaps are often associated with cluster stability. Considering the binding energies of $Au_{13}(SCH_3)_{12}$ clusters of different geometries given by,

$$E_{B.E} = E(Au_{13}) + 12 * E(SCH_3) - E[Au_{13}(SCH_3)_{12}] \quad (1)$$

we get a largest relative binding energy ($\Delta E_{B.E}$) for icosahedral $Au_{13}(SCH_3)_{12}$ (up to 3.90 eV, versus 0.49 eV for distorted-planar, 0 eV for flake, and 1.34 eV for cuboctahedral) among the four isomers. Besides, Fig. 2C shows a second largest HOMO-LUMO gap (up to 1.36 eV) for the icosahedral Au_{13} $(SCH_3)_{12}$. These results may indicate an increasing stability of the icosahedral Au_{13} MPCs compared with other three geometries when linked with the protected ligands. It is worth noting that the UV–Vis absorption profiles (Fig. S4c in ESI) remain unchanged after 2 h and one month, also demonstrating photo-stabilization and chemical stability of the Au_{13} MPCs.

While stabilities of MPCs are often understood using the conceptual framework of superatoms validated in the gas phase on a basis of electronic shells [48], a pending question is that how to rationalize the planar-to-nonplanar turnover occurred in this small gold cluster. Wang [29] found that gold atoms in forming clusters exhibit covalent bonding analogous to boron clusters, which rationalizes why small gold clusters such as Au_{13} prefer a planar structure in the gas phase. However, considering that the bond strength for an Au—Au bond (~2.27 eV) is less than that of an Au—S bond (4.34 eV), it is feasible for structural rearrangement of Au_{13} in the presence of —SH radicals. What's more, the existence of binary thiolates benefits to initialize a distortion of charge distribution and then geometric structure due to the minor difference of —SH bonds in glutathione and penicillamine. In view of this, we then compared the shapes of HOMO orbital of Au_{13} core and $Au_{13}(SCH_3)_{12}$ cluster to see whether thiolate ligands affect Au_{13} core orbitals. Note that HOMOs of Au_{13} core and $Au_{13}(SCH_3)_{12}$ cluster differ from each other (Fig. S4c, Supporting Information), indicating non-neglectable interactions between Au and S atoms. In order to reveal orbital interactions and the stability of the icosahedral structured $Au_{13}(SCH_3)_{12}$, we have plotted the natural bond orbital (NBO) donor-acceptor overlaps, as shown in Fig. 2D, where the second-order perturbation stabilization energies in icosahedral $Au_{13}(SCH_3)_{12}$ cluster is also labeled. The donor-acceptor interaction energy corresponds to the strength of the orbital overlaps in such

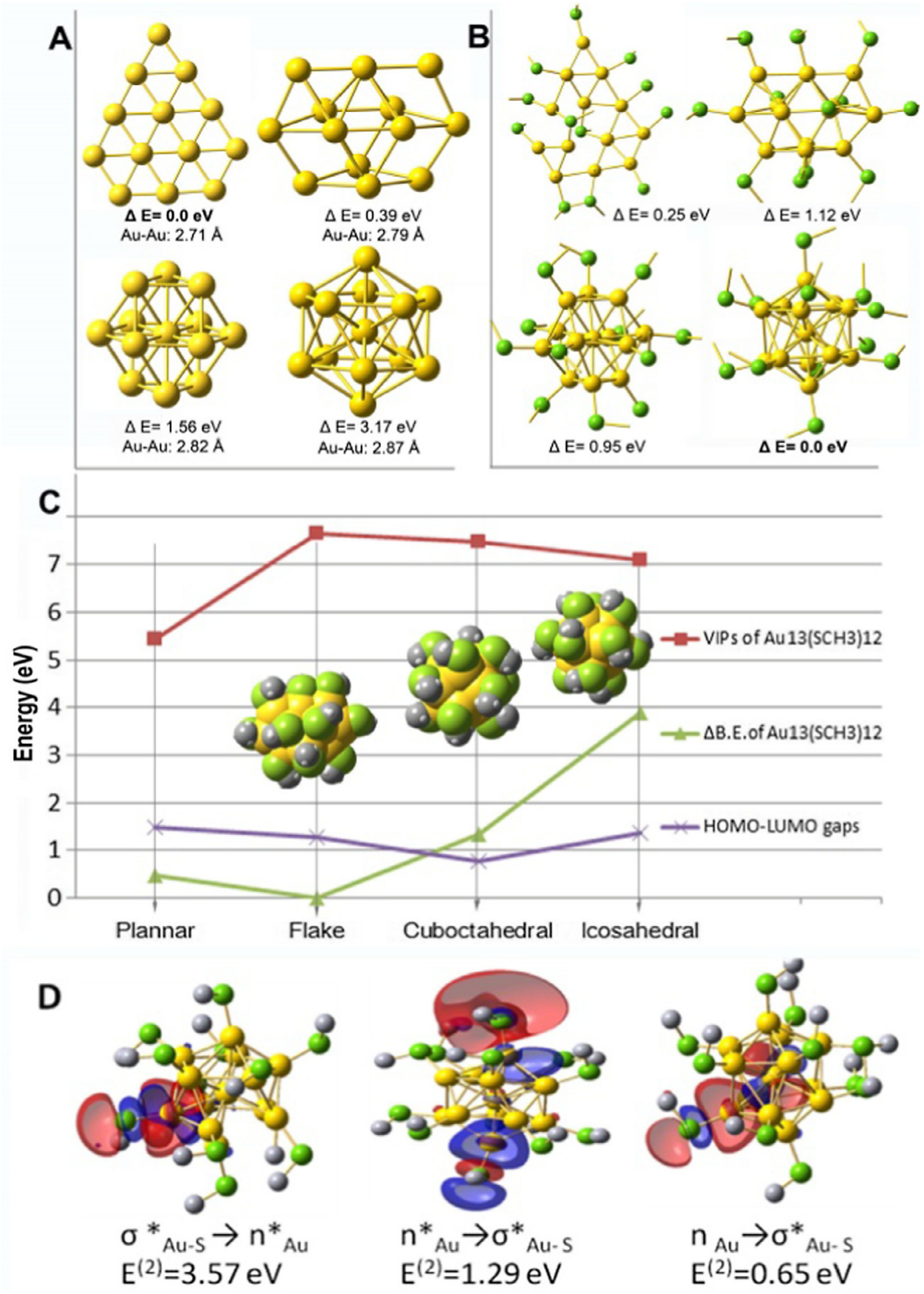

Fig. 2. Isomers of bare Au_{13} (A) and $Au_{13}(SCH_3)_{12}$ cluster (B) for planar, flake, cuboctahedral, and icosahedral geometries. (C) Vertical ionization potentials, binding energy ($\Delta E_{B.E}$) and HOMO-LUMO gaps of the four isomers of $Au_{13}(SCH_3)_{12}$. The $-CH_3$ groups in the structures shown in B are omitted. (D) NBO donor-acceptor overlaps and second-order perturbation stabilization energies ($E^{(2)}$) in $Au_{13}(SCH_3)_{12}$: n(Au) → σ*(Au—S), n*(Au) → σ*(Au—S), and σ*(Au—S) → n*(Au). The hydrogen atoms are omitted.

complexes [49]. Typically, the donor-acceptor overlaps exist within the antibonding lone pair of Au atom, n* (Au), lone pair of Au atom, n (Au), and antibonding orbital of Au—S bond, σ* (Au—S), antibonding orbital of C—S bond, σ* (C—S), such as σ*(Au—S) → n*(Au), n*(Au) → σ*(Au—S) and n(Au) → σ*(Au—S). It is important to note that the dominant donor-acceptor charge transfer interactions belong to adjacent subsystems. As shown in Fig. 2D and Fig. S6 in ESI, the large second-order perturbation stabilization energies dominate strong donor-acceptor interactions, indicating that the charge transfer between the ligands and Au core atoms plays an important role in stabilizing the $Au_{13}(SG)_5(PA)_7$ clusters.

Fluorescence experiments have shown that the water-soluble Au_{13} MPCs exhibit an intense fluorescence emission package at 690 nm (the excitation wave length λex = 320 nm), which gives

rise to an important application potential in fluorescence chemosensor for ions detection and bio-imaging. Experiments show that the changes of excitation did not affect the fluorescence emission (Fig. S2c, ESI). Therefore, in order to avoid the appearance of the double frequency peak at 640 nm, we choose the 550 nm as the excitation wavelength. Herewith we have made an effort on this and found high sensitivity at the presence of Cu^{2+} and Fe^{3+} ions. As shown in Fig. 3A, cationic ions Al^{3+}, Cd^{2+}, Ca^{2+}, Cr^{3+}, Cu^{2+}, Pb^{2+}, Mn^{2+}, Na^{+}, Ni^{2+} and Zn^{2+} are found to enhance the nascent fluorescence to different extents, while the addition of Fe^{3+} and Cu^{2+} ions to $Au_{13}(SG)_5(PA)_7$ MPCs results in fluorescence quenching. We have also conducted fluorescence titration experiments for Au MPCs by adding Fe^{3+} and Cu^{2+} ions of varying concentrations, respectively (Fig. 3B and 3C). Fluorescence intensity at 690 nm decreases remarkably with increasing concentrations of Fe^{3+}/Cu^{2+} ions, and upon further increase of the Fe^{3+}/Cu^{2+} ions concentration, fluorescence emission tends to be quenched completely. Based on fluorescence titration results, linear regression curves are plotted between relative fluorescence intensity and ion concentrations (Fig. S7, ESI), and the detection limits of Au_{13} MPCs were deduced 1.38 μM for Fe^{3+} and 3.89 μM for Cu^{2+}, respectively, which is comparable with the previously reported investigations. To validate the

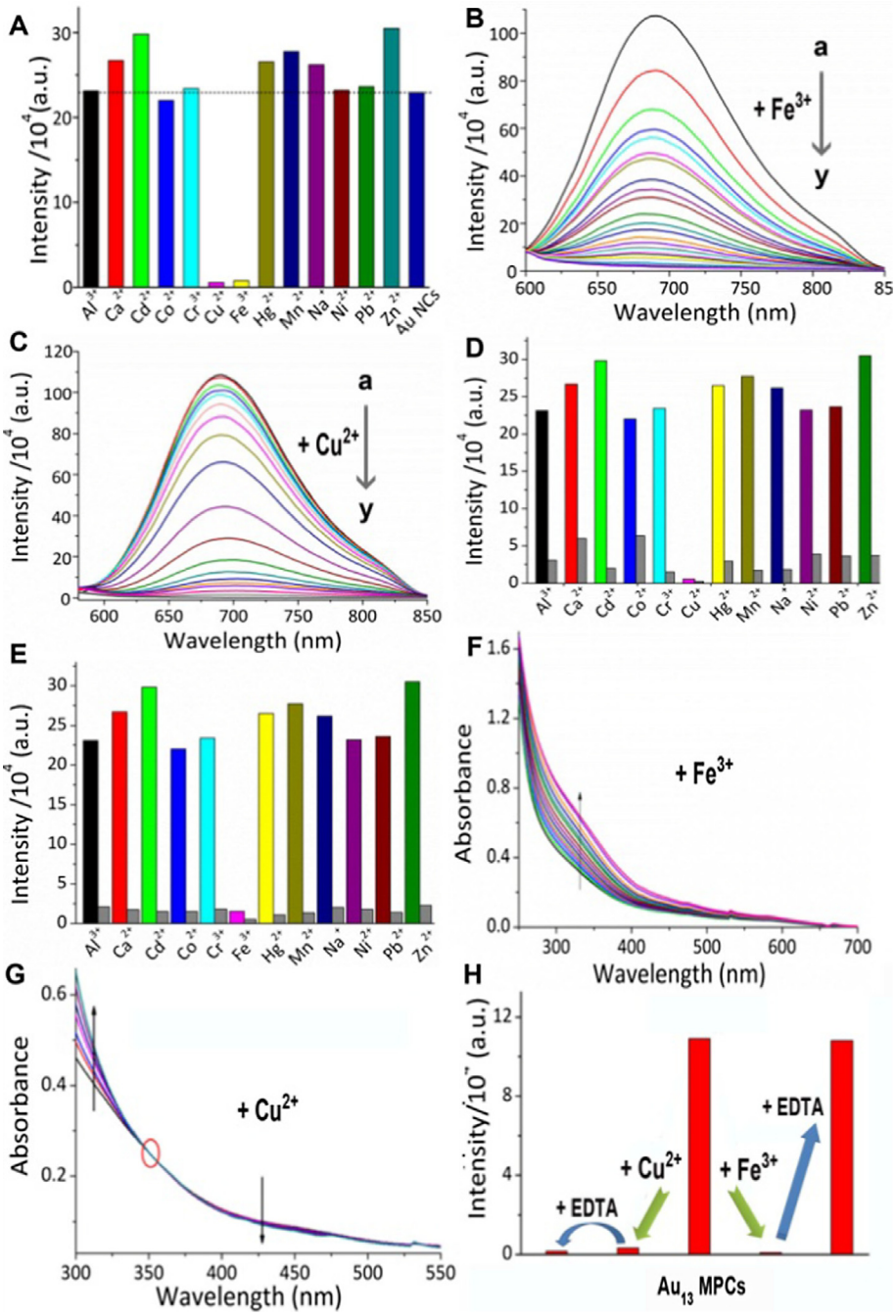

Fig. 3. (A) Fluorescence responses of Au_{13} cluster in H_2O to metal cations. (B) Fluorescence titration profiles (λ_{ex} = 550 nm) of Au_{13} MPCs (10 μg/mL) in the presence of increasing amounts of Fe^{3+} (0–33 μM) in H_2O. (C) Fluorescence titration profiles (λ_{ex} = 550 nm) of Au_{13} MPCs (10 μg/mL) in the presence of increasing amounts of Cu^{2+} (0–21 μM) in H_2O. (D/E) Fluorescence intensity at 690 nm of Au_{13} MPCs with Fe^{3+} and Cu^{2+} in the presence of various interferential metal ions. (F/G) UV–Vis titration spectra of Au_{13} MPCs in the presence of increasing amounts of Fe^{3+} and Cu^{2+}. (H) Fluorescence intensity changes of Au_{13} MPCs before and after adding Fe^{3+} and Cu^{2+} ions and subsequently EDTA respectively.

high selectivity of Au_{13} MPCs for the detection of Fe^{3+} and Cu^{2+} in practice, competitive fluorescence titration was carried out. Au_{13} MPCs was treated with 1.0 equiv of Fe^{3+}/Cu^{2+} in the presence of 1.0 equiv of other metal ions. As shown in Fig. 3D and 3E, there is no interference with the detection of Fe^{3+}/Cu^{2+} in the presence of all other metal ions, indicating high selectivity and sensitivity of the Au_{13} MPCs towards Fe^{3+} and Cu^{2+} ions in H_2O.

In order to distinguish cationic Fe^{3+} from Cu^{2+}, we have studied the ratiometric absorption behaviors for Fe^{3+} and Cu^{2+}, respectively, as given in Fig. 3F and 3G, where different ratiometric absorption behaviors for Fe^{3+} and Cu^{2+} are addressed. It is noteworthy that the position of the absorption peak displays rare changes, but the intensity increased gradually with the Fe^{3+} ions increasing. However, the gradual addition of Cu^{2+} ions differs distinctly from that of Fe^{3+} ions. An isobestic point emerges at ~350 nm with Cu^{2+} concentration increasing (in the lower concentration range). Considering that more gradual addition of Cu^{2+} ions in a higher concentration range (Fig. S11, ESI) still allows the absorption intensity increasing gradually just like that of Fe^{3+} ions, we have further applied masking method to differentiate Fe^{3+} from Cu^{2+} in case of high concentration samplings. In addition, we used masking method to further differentiate Fe^{3+} from Cu^{2+}, a chelating agent (EDTA) is chosen in this study. As shown in Fig. 3H, where the fluorescence intensity of Au_{13} MPCs returns to 98 % of its initial value when EDTA is added to the non-fluorescent sample (quenched by anterior Fe^{3+}); in sharp contrast, the response of Cu^{2+}-added MPCs is dumb. From this result, it is supposed that $Au_{13}(SG)_5(PA)_7$ MPCs have a higher binding affinity towards Cu^{2+}, which prohibits the release of Cu^{2+} from the aggregated system. Considering the larger formation constant "log K (Fe^{3+}–EDTA) = 25.10", versus "log K (Cu^{2+}–EDTA) = 18.80", as well as likely lower binding affinity of the Au_{13} MPCs towards Fe^{3+}, the presence of EDTA could withdraw the Fe^{3+} ions hence allowing for recovery of fluorescence.

In general, fluorescence quenching could be simply caused by energy transfer or static quenching in forming nonfluorescent complexes. But the presence of multiple chemicals may perplex this process. To provide an indepth insight into the sensing mechanism, we have conducted a check on the ^1H NMR experiments and TEM characterizations of Au_{13} MPCs before and after the addition of Fe^{3+} and Cu^{2+} ions. As shown in Fig. S8 (ESI), when gradually adding Fe^{3+} and Cu^{2+} ions to the Au_{13} MPCs, all proton signals disappear and finally only a solvent D_2O peak exists at 4.79 ppm. With further increasing of Fe^{3+} and Cu^{2+} ion concentrations, there are brown precipitates out of the solution. From TEM observation, the nascent Au_{13} MPCs display decent monodispersity (Fig. S9, ESI); however, there are aggregation patterns at the presence of Fe^{3+} and Cu^{2+} ions. At a comparison of XPS patterns of the Au 4f core-level for the Au_{13} MPCs before and after reacting with Fe^{3+} and Cu^{2+} ions (Fig. S10, ESI), a minor shift towards high-energy region was observed upon addition of Fe^{3+} or Cu^{2+} ions to the Au_{13} MPCs, suggesting neglectable energy transfer between the ions and Au_{13} MPCs, resulting in aggregation-induced fluorescence quenching (AIFQ), which profits from the interaction of hard acid Fe^{3+} or Cu^{2+} ions with the multiple hard base —NH and —O atoms presenting in several —SG and —PA ions. In brief, the chemosensing mechanism is written as,

$$\begin{aligned} &2Au_n(SR)_x^- + Cu^{2+} \rightarrow [Au_n(RS)_x \cdots Cu \cdots (SR)_xAu_n]^0 \\ &\quad \overset{+EDTA}{\Rightarrow} [Au_n(RS)_xCu(SR)_xAu_n]^0 \\ &3Au_n(SR)_x^- + Fe^{3+} \rightarrow [Au_n(RS)_x \cdots Fe \cdots [(SR)_xAu_n]_2]^0 \\ &\quad \overset{+EDTA}{\Rightarrow} 3Au_n(SR)_x^0 + [Fe \cdot EDTA]^0 \end{aligned} \quad (2)$$

Having depicted the excellent selectivity and highly-sensitive differentiate analysis of Au_{13} MPCs towards Fe^{3+} and Cu^{2+} ions in water, we have endeavored to explore its potential application in living cell bioimaging (for details, see the experimental section in ESI). We have tested the toxicity of the as-prepared Au MPCs to SH-SY5Y cells (Fig. 4A). Based on the MTT assay results, the cellular viabilities are estimated nearly 92%, confirming that the as-prepared Au MPCs are almost not toxic for SH-SY5Y cells. The SH-SY5Y cells were incubated with Au MPCs for 2 h firstly, and then treated with Fe^{3+} and Cu^{2+} ions for 30 min, respectively. As shown in Fig. 4B, the cells only incubated with Au MPCs display strong fluorescence, while the strong red fluorescence quenches in cells when exposed to aqueous solution of Fe^{3+} and Cu^{2+} ions. Then, the fluorescence intensity of gold nanoclusters recovers when further incubated with EDTA for 10 min after quenching by Fe^{3+}, while almost no changes toward Cu^{2+} upon the addition of EDTA. These results revealed that the $Au_{13}(SG)_5(PA)_7$ MPCs are capable of detecting and distinguishing intracellular Fe^{3+} and Cu^{2+} ions by cell imaging.

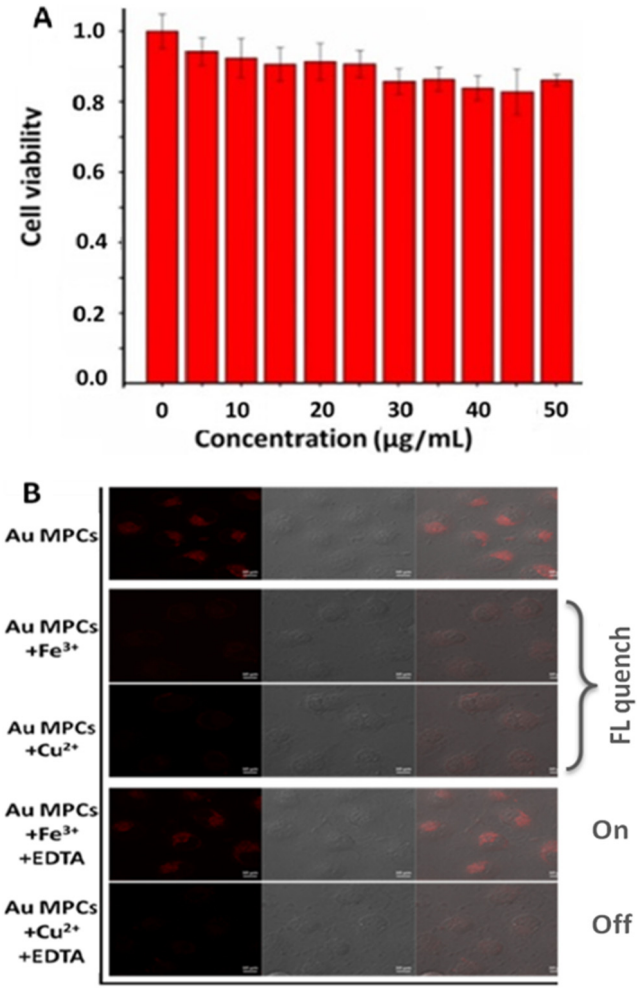

Fig. 4. (A) Cell viability values estimated by MTT proliferation test versus concentrations of Au_{13} clusters after 24 h incubation at 37 °C. (B) Confocal fluorescence images of only Au_{13} clusters, addition of Fe^{3+}/Cu^{2+} ions and addition of Fe^{3+}/Cu^{2+} ions + EDTA in SH-SY5Y cells in the fluorescence (left), bright (middle) and overlay (right) field, respectively.

4. Conclusions

In conclusion, we report here a successful synthesis procedure of Au_{13} MPCs protected by binary thiolates. From the mass spectrometry analysis and spectral measurements, the component and composition of this cluster was determined as $Au_{13}(SG)_5(PA)_7$ where the total 12 ligands work as a fully protected monolayer by

forming Au—S bonds on 12 Au atoms except the center one. Further, the lowest-energy structure of this gold cluster was determined utilizing first-principles calculations within both VASP and Gaussian software package, verifying the planar-to-nonplanar turnover occurred in small gold cluster. Also found was that, the as-prepared Au_{13} MPCs take on red fluorescence and enhanced stability due to the donor-acceptor orbital interactions between the gold and chemisorbed sulphur. Utilizing this fluorescent Au_{13} MPCs as chemosensor, we have obtained the detection and differentiation of Fe^{3+} and Cu^{2+} ions with high selectivity and sensitivity, and successfully applied for bio-imaging and intracellular detection of Fe^{3+} and Cu^{2+} ions pertaining to potential applications.

Acknowledgements

This work was financially supported by CAS Key Research Project of Frontier Science (Y62A0412B1), CAS Instrument development project (Y5294512C1), and Frontier Cross Project of national laboratory for molecular sciences (051Z011BZ3). Z. Luo acknowledges the national Thousand Youth Talents Program (Y3297B1261). C.H. and W.L. acknowledge the National Natural Science Foundation of China (21321002, 21225315).

Appendix A. Supplementary material

Supplementary data associated with this article can be found, in the online version, at http://dx.doi.org/10.1016/j.cplett.2017.03.036.

References

[1] Z. Wu, E. Lanni, W. Chen, M.E. Bier, D. Ly, R. Jin, J. Am. Chem. Soc. 131 (2009) 16672.
[2] G. Schmid, Chem. Soc. Rev. 37 (2008) 1909.
[3] C.J. Ackerson, P.D. Jadzinsky, G.J. Jensen, R.D. Kornberg, J. Am. Chem. Soc. 128 (2006) 2635.
[4] G. Ramakrishna, O. Varnavski, J. Kim, D. Lee, T. Goodson, J. Am. Chem. Soc. 130 (2008) 5032.
[5] P.D. Jadzinsky, G. Calero, C.J. Ackerson, D.A. Bushnell, R.D. Kornberg, Science 318 (2007) 430.
[6] Y. Song, F. Fu, J. Zhang, J. Chai, X. Kang, P. Li, S. Li, H. Zhou, M. Zhu, Angew. Chem. Int. Ed. 54 (2015) 8430.
[7] C.M. Chang, C. Cheng, C.M. Wei, J. Chem. Phys. 128 (2008).
[8] H.F. Qian, W.T. Eckenhoff, Y. Zhu, T. Pintauer, R.C. Jin, J. Am. Chem. Soc. 132 (2010) 8280.
[9] C.J. Zeng, H.F. Qian, T. Li, G. Li, N.L. Rosi, B. Yoon, R.N. Barnett, R.L. Whetten, U. Landman, R.C. Jin, Angew. Chem. Int. Ed. 51 (2012) 13114.
[10] D. Crasto, S. Malola, G. Brosofsky, A. Dass, H. Hakkinen, J. Am. Chem. Soc. 136 (2014) 5000.
[11] H.Y. Yang, Y. Wang, A.J. Edwards, J.Z. Yan, N.F. Zheng, Chem. Commun. (Cambridge, U. K.) 50 (2014) 14325.
[12] M.W. Heaven, A. Dass, P.S. White, K.M. Holt, R.W. Murray, J. Am. Chem. Soc. 130 (2008) 3754.
[13] M. Zhu, C.M. Aikens, F.J. Hollander, G.C. Schatz, R. Jin, J. Am. Chem. Soc. 130 (2008) 5883.
[14] C.J. Zeng, C. Liu, Y.X. Chen, N.L. Rosi, R.C. Jin, J. Am. Chem. Soc. 136 (2014) 11922.
[15] X.K. Wan, Z.W. Lin, Q.M. Wang, J. Am. Chem. Soc. 134 (2012) 14750.
[16] Y. Chen, C. Zeng, C. Liu, K. Kirschbaum, C. Gayathri, R.R. Gil, N.L. Rosi, R. Jin, J. Am. Chem. Soc. 137 (2015) 10076.
[17] Y. Shichibu, K. Suzuki, K. Konishi, Nanoscale 4 (2012) 4125.
[18] T. Watanabe, K. Koyasu, T. Tsukuda, J. Phys. Chem. C 119 (2015) 10904.
[19] R. Burgert, H. Schnockel, Chem. Commun. (Camb) (2008) 2075.
[20] O. Gantassi, C. Menakbi, N. Derbel, H. Guesmi, T. Mineva, J. Phys. Chem. C 119 (2015) 3153.
[21] J. Chen, H. Zhang, X. Liu, C. Yuan, M. Jia, Z. Luo, J. Yao, Phys. Chem. Chem. Phys. 18 (2016) 7190.
[22] Z. Luo, G.U. Gamboa, J.C. Smith, A.C. Reber, J.U. Reveles, S.N. Khanna, A.W. Castleman Jr., J. Am. Chem. Soc. 134 (2012) 18973.
[23] M. Sugiuchi, Y. Shichibu, T. Nakanishi, Y. Hasegawa, K. Konishi, Chem. Commun. (Cambridge, U.K.) 51 (2015) 13519.
[24] G. Shafai, S. Hong, M. Bertino, T.S. Rahman, J. Phys. Chem. C 113 (2009) 12072.
[25] J.L. Wang, G.H. Wang, J.J. Zhao, Phys. Rev. B 66 (2002) 035418.
[26] J. Zhao, J.L. Yang, J.G. Hou, Phys. Rev. B 67 (2003) 085404.
[27] L. Xiao, B. Tollberg, X.K. Hu, L.C. Wang, J. Chem. Phys. 124 (2006) 114309.
[28] M. Gruber, G. Heimel, L. Romaner, J.-L. Bredas, E. Zojer, Phys. Rev. B 77 (2008) 165411.
[29] L.S. Wang, Phys. Chem. Chem. Phys. 12 (2010) 8694.
[30] Y. Shichibu, K. Konishi, Small 6 (2010) 1216.
[31] Y. Negishi, K. Nobusada, T. Tsukuda, J. Am. Chem. Soc. 127 (2005) 5261.
[32] Y.Y. Yang, S.W. Chen, Nano Lett. 3 (2003) 75.
[33] M.Z. Zhu, W.T. Eckenhoff, T. Pintauer, R.C. Jin, J. Phys. Chem. C 112 (2008) 14221.
[34] Z. Luo, C.J. Grover, A.C. Reber, S.N. Khanna, A.W. Castleman, J. Am. Chem. Soc. 135 (2013) 4307.
[35] Z. Luo, A.C. Reber, M. Jia, W.H. Blades, S.N. Khanna, A.W. Castleman Jr., Chem. Sci. 7 (2016) 3067.
[36] Y. Zheng, Z. Yang, J.Y. Ying, Adv. Mater. (Weinheim, Ger.) 19 (2007) 1475.
[37] M. Green, H. Harwood, C. Barrowman, P. Rahman, A. Eggeman, F. Festry, P. Dobson, T. Ng, J. Mater. Chem. 17 (2007) 1989.
[38] J. Li, X. Hong, Y. Liu, D. Li, Y.W. Wang, J.H. Li, Y.B. Bai, T.J. Li, Adv. Mater. (Weinheim, Ger.) 17 (2005) 163.
[39] A. Shavel, N. Gaponik, A. Eychmuller, ChemPhysChem 6 (2005) 449.
[40] X. Yuan, B. Zhang, Z. Luo, Q. Yao, D.T. Leong, N. Yan, J. Xie, Angew. Chem. Int. Ed. 53 (2014) 4623.
[41] N. Nishida, H. Yao, K. Kimura, Langmuir 24 (2008) 2759.
[42] T.U.B. Rao, B. Nataraju, T. Pradeep, J. Am. Chem. Soc. 132 (2010) 16304.
[43] T. Udayabhaskararao, M.S. Bootharaju, T. Pradeep, Nanoscale 5 (2013) 9404.
[44] J.W.A. Vandervelden, F.A. Vollenbroek, J.J. Bour, P.T. Beurskens, J.M.M. Smits, W.P. Bosman, Rec. Trav. Chim.-J. R. Neth. Chem. Soc. 100 (1981) 148.
[45] C.E. Briant, B.R.C. Theobald, J.W. White, L.K. Bell, D.M.P. Mingos, A.J. Welch, J. Chem. Soc.-Chem. Commun. (1981) 201.
[46] C.E. Briant, B.R.C. Theobald, J.W. White, L.K. Bell, D.M.P. Mingos, J. Chem. Soc., Chem. Commun. (1981) 201.
[47] G. Shafai, S.Y. Hong, M. Bertino, T.S. Rahman, J. Phys. Chem. C 113 (2009) 12072.
[48] Z. Luo, A.W. Castleman Jr., Acc. Chem. Res. 47 (2014) 2931.
[49] Z. Zhang, J. Shen, N. Jin, L. Chen, Z. Yang, Comput. Theo. Chem. 999 (2012) 48.